JOURNAL OF AIRCRAFT
Vol. 40, No. 3, May–June 2003

Three-Dimensional Transonic Aeroelasticity Using Proper Orthogonal Decomposition-Based Reduced-Order Models

Jeffrey P. Thomas,* Earl H. Dowell,† and Kenneth C. Hall‡
Duke University, Durham, North Carolina 27708-0300

The proper orthogonal decomposition (POD-) based reduced-order modeling technique for modeling unsteady frequency-domain aerodynamics is developed for a large-scale computational model of an inviscid flow transonic wing configuration. When the methodology is used, it is shown that a computational fluid dynamic model with over three-quarters of a million degrees of freedom can be reduced to a system with just a few dozen degrees of freedom, while still retaining the accuracy of the unsteady aerodynamics of the full system representation. Furthermore, POD vectors generated from unsteady flow solution snapshots based on one set of structural mode shapes can be used for different structural mode shapes so long as solution snapshots at the endpoints of the frequency range of interest are included in the overall snapshot ensemble. Thus, the snapshot computation aspect of the method, which is the most computationally expensive part of the procedure, does not have to be fully repeated as different structural configurations are considered.

Nomenclature

$\boldsymbol{A}$	=	matrix defining homogeneous part of discretized fluid dynamic operator
$\mathcal{A}$	=	reduced-order form of $\boldsymbol{A}$
AR	=	aspect ratio equal to wing span squared/wing area
$\boldsymbol{B}$	=	matrix relating modal structural motion coordinates $\boldsymbol{\xi}$ to CFD boundary conditions
$\mathcal{B}$	=	reduced-order form of $\boldsymbol{B}$
b, c	=	semichord and chord, respectively
$\boldsymbol{C}$	=	matrix relating unsteady flow $\boldsymbol{q}$ to generalized forces $\boldsymbol{C}_{\mathcal{Q}}$ acting on wing
$\mathcal{C}$	=	reduced-order form of $\boldsymbol{C}$
$\boldsymbol{C}_{\mathcal{Q}}$	=	vector of nondimensional generalized forces
$\boldsymbol{I}$	=	identity matrix
j	=	$\sqrt{(-1)}$
M	=	number of structural modes
$\mathcal{M}$	=	generalized mass matrix
M_∞	=	freestream Mach number
$\bar{m}$	=	mass of wing
N	=	number of degrees of freedom of computational fluid dynamics model
N_P	=	number of proper orthogonal decomposition (POD) vectors
N_S	=	total number of solution snapshot vectors
p	=	unsteady pressure
$\boldsymbol{Q}, \boldsymbol{q}$	=	vectors for steady and small-disturbance flow solutions
$\mathcal{Q}$	=	vector of generalized forces
q_∞	=	freestream dynamic pressure
r	=	magnitude of reduced Laplace variables $\bar{s}$
$\bar{s}$	=	complex reduced frequency Laplace variable, $j\bar{\omega}$
U_∞	=	freestream velocity
V	=	reduced velocity, $U_\infty/\sqrt{(\mu)}\omega_\alpha b$
$v, \boldsymbol{v}$	=	reduced-order fluid dynamic variable and vector of reduced-order fluid dynamic variables
$\bar{v}$	=	volume of a truncated cone having streamwise root chord as lower base diameter, streamwise tip chord as upper base diameter, and wing half span as height
α_0	=	airfoil or wing root steady flow angle of attack
θ	=	angle made by reduced Laplace variable $\bar{s}$ in complex frequency plane, $\bar{s} = re^{j\theta}$
λ_t	=	wing taper ratio, c_t/c_r
μ	=	mass ratio for wing configuration, $\bar{m}/\rho_\infty \bar{v}$
$\xi, \boldsymbol{\xi}$	=	structural coordinate and vector of structural coordinates
ρ_∞	=	freestream density
$\phi, \boldsymbol{\Phi}$	=	POD vector and matrix of POD vectors
ψ	=	structural mode shape
$\boldsymbol{\Omega}$	=	matrix with structural frequency ratios squared along main diagonal, that is, $(\omega_1/\omega_\alpha)^2, \ldots, (\omega_M/\omega_\alpha)^2$
ω	=	frequency
ω_α	=	wing first torsional mode natural frequency
$\bar{\omega}$	=	reduced frequency, $\omega c/U_\infty$ (for airfoil) and $\omega b/U_\infty$ for wing

Subscripts/Superscripts

f	=	flutter, that is neutral stability, condition
H	=	Hermitian transpose
r, t	=	root and tip, respectively

Presented as Paper 2001-0855 at the AIAA/ASME/ASCE/AHS/ASC 42nd Structures, Structural Dynamics and Materials Conference, Seattle, WA, 16 April 2001; received 1 May 2001; revision received 5 September 2002; accepted for publication 6 September 2002.

*Research Assistant Professor, Department of Mechanical Engineering and Materials Science. Member AIAA.

†J. A. Jones Professor, Department of Mechanical Engineering and Materials Science, and Dean Emeritus, School of Engineering. Fellow AIAA.

‡Professor and Department Chairperson, Department of Mechanical Engineering and Materials Science. Associate Fellow AIAA.

Introduction

IN the following, we demonstrate how the recently devised proper orthogonal decomposition- (POD-) based reduced-order modeling (ROM) technique[1–3] can be used to model unsteady aerodynamic and aeroelastic characteristics of three-dimensional inviscid transonic wing configurations. Although an incompressible vortex lattice fluid model[1] and transonic Euler computational fluid dynamic (CFD) models[2,3] have been previously studied, these initial demonstrations of the POD/ROM method have been for two-dimensional airfoil configurations with at most two structural degrees of freedom, for example, plunge and pitch.

When the POD/ROM technique is extended to three dimensions, two primary issues are of concern. First, the size of the CFD model will in general be at least an order of magnitude greater than for two dimensions. Whereas a typical CFD model for a realistic two-dimensional configuration might have on the order of tens or even hundreds of thousands of degrees of freedom (DOF), a CFD model

for a three-dimensional configuration might easily have on the order of hundreds of thousands if not millions or more DOF. In two dimensions, we have found that very accurate ROMs with on the order of only a few dozen DOF can be devised using the POD/ROM methodology. Thus, a first issue to address has been whether or not one can also generate accurate ROMs in three dimensions which also require at most a few dozen DOF.

The second concern is, for any variation of the structural properties of a given wing under consideration, will a completely new ensemble of solution vector "snapshots" have to be computed to devise an accurate POD/ROM. A basic aspect of the POD/ROM method is that an ensemble of solution vectors is first assembled by computing unsteady CFD solutions at a number of discrete frequencies within a frequency range of interest for the unsteady structural motions that are also of interest. In two dimensions, this step is relatively straightforward because one only has to consider a few possible motions, for example, pitch and plunge.

In three dimensions, however, the wing vibratory mode shapes will be different for each different structural configuration of a given wing. As such, there can be a substantial number of unsteady motions (or at least a number of motions equivalent to the number of DOF of the discrete structural model) one must consider. Thus, the second concern about extending the POD/ROM to three-dimensions has been whether or not it is necessary to compute a completely different ensemble of solution snapshots for every possible structural configuration. For example, say one computes solution snapshots for a given wing configuration based on the wing's particular vibratory mode shapes to develop a POD/ROM to model the configuration's aeroelastic characteristics. The question is, if the structural definition of the wing changes, does one have to compute a whole new ensemble of solution snapshots for the different set of vibratory structural mode shapes.

Fortunately in addressing these two issues, as will be shown in the following, we have found that accurate POD/ROMs with just a few dozen degrees of freedom can in fact be created for realistic transonic three-dimensional configurations. This is true even for a CFD model that is easily an order of magnitude larger than anything we have previously studied in two dimensions. Furthermore, we have discovered that a "fundamental" ensemble of solution snapshots, based on wing motions that need not be identical to the structural modes under consideration, can be assembled as a first step. Accurate POD/ROMs for a given wing configuration can then be created by simply adding to this fundamental ensemble, the snapshots corresponding to actual wing structural modal motions solely at the frequencies corresponding to the endpoints of the frequency range of interest. In general, these two snapshots prove to be sufficient to "lock in" the conditions corresponding to the particular structural motion, and indeed this fundamental ensemble of solution snapshots is sufficient to reveal the unsteady dynamics of the fluid dynamic model. Consequently, this fundamental ensemble of snapshots can be used again and again even as the structural model changes, and the computational cost of having to compute an entirely new snapshot ensemble for every new structural configuration is, thus, greatly reduced.

POD/ROM Methodology

In the following, we will be considering inviscid transonic three-dimensional flows and, more specifically, linearized (about some nonlinear background steady flow) unsteady frequency-domain CFD solutions to the Euler equations. The POD/ROM procedure can be applied in principle to any conventional CFD method. The CFD method we have employed for the present analysis is a variant of Ni's[4] approach to the standard Lax–Wendroff method. The frequency-domain CFD method in effect represents a linear system formulation of the unsteady fluid dynamic model, that is,

$$\boldsymbol{Aq} = -\boldsymbol{B\xi} \tag{1}$$

where $\boldsymbol{q}$ is the N-dimensional vector (N is the number of mesh points times the number of dependent flow variables) of dependent unsteady flow variables at each mesh point in the CFD domain and $\boldsymbol{\xi} = \{\xi_1, \ldots, \xi_M\}^T$ is the M-dimensional vector of modal coordinates for the structural model. $\boldsymbol{A}$ is the $N \times N$ fluid dynamic influence matrix, and $\boldsymbol{B}$ is the $N \times M$ matrix that relates the flow solver boundary conditions to each particular structural mode shape. $\boldsymbol{A}$ and $\boldsymbol{B}$ are both functions of the background flow $\boldsymbol{Q}$ and unsteady frequency ω. The structural equations for the wing configuration can be written as

$$\boldsymbol{D\xi} = -\boldsymbol{Cq} \tag{2}$$

where $\boldsymbol{D}$ is the $M \times M$ structural influence matrix, which in the case of the case of a swept delta wing configuration can be expressed as

$$\boldsymbol{D\xi} = k_w \boldsymbol{\mathcal{M}}[-\bar{\omega}^2 \mu \boldsymbol{I} + (1/V^2)\boldsymbol{\Omega}]\boldsymbol{\xi} \tag{3}$$

where k_w is a constant dependent on the wing shape and overall mass given by

$$k_w = \frac{\pi \mathrm{AR}(1+\lambda_t)\left(1+\lambda_t+\lambda_t^2\right)}{6\bar{m}} \tag{4}$$

$\boldsymbol{C}$ is the $M \times N$ matrix that represents the discrete integration operator used to obtain the generalized forces associated with each structural mode shape and unsteady flow $\boldsymbol{q}$, that is,

$$\boldsymbol{Cq} = -\boldsymbol{C}_{\mathcal{Q}} \tag{5}$$

where $\boldsymbol{C}_{\mathcal{Q}} = \boldsymbol{\mathcal{Q}}/q_\infty c_r^2$ (where $\boldsymbol{\mathcal{Q}} = \{\mathcal{Q}_1, \ldots, \mathcal{Q}_M\}^T$) is the vector of frequency-dependent generalized aerodynamic force coefficients acting on the wing. The generalized aerodynamic force coefficients can also be written in matrix form as

$$\boldsymbol{C}_{\mathcal{Q}} = \underbrace{\left[\frac{\partial C_{\mathcal{Q}_i}}{\partial \xi_j}\right]}_{M \times M} \xi = [E_{i,j}]\,\boldsymbol{\xi} \tag{6}$$

where $[\partial C_{\mathcal{Q}_i}/\partial \xi_j]$ is the $M \times M$ matrix of aerodynamic transfer functions ($\partial C_{\mathcal{Q}_i}/\partial \xi_j$ being the coefficient of the ith generalized force due to the jth structural modal coordinate) that we wish to approximate with the ROM strategy.

Coupling Eqs. (1) and (2), for example,

$$\begin{bmatrix} \boldsymbol{A} & \boldsymbol{B} \\ \boldsymbol{C} & \boldsymbol{D} \end{bmatrix} \begin{Bmatrix} \boldsymbol{q} \\ \boldsymbol{\xi} \end{Bmatrix} = \begin{Bmatrix} \boldsymbol{0} \\ \boldsymbol{0} \end{Bmatrix} \tag{7}$$

yields the aeroelastic system of equations, which for nontrivial $\boldsymbol{q}$ and $\boldsymbol{\xi}$, represents an eigenvalue problem with $\bar{\omega}$ being the eigenvalue. Any eigenvalues with a positive real part imply the aeroelastic system is unstable.

The problem with constructing and solving this eigenvalue problem is that $\boldsymbol{A}$ is simply too large for typical CFD models of realistic configurations. As mentioned in the Introduction, N can easily be on the order of 10^4 or 10^5 for two-dimensional configurations, and on the order of 10^5–10^6 or even more for three-dimensional configurations. For such large models, even attempting to set up and assemble $\boldsymbol{A}$ is well beyond the memory limits of the largest modern computers.

The basic premise of the POD/ROM technique is that we assume the unknown unsteady flowfield solution vector $\boldsymbol{q}$ can be expressed as a Ritz type expansion of the form

$$\boldsymbol{q} \approx \sum_{n=1}^{N_P} v_n \boldsymbol{\phi}_n, \qquad N_P \ll N \tag{8}$$

where v_n is a generalized coordinate sometimes referred to as an augmented aerodynamic state variable and $\boldsymbol{\phi}_n$ is the corresponding Ritz vector. N_P is the number of Ritz vectors, which in the following

will be POD vectors, used in the expansion. Equation (8) can also be written in matrix form as

$$\boldsymbol{q} = \boldsymbol{\Phi v}, \quad \text{where} \quad \boldsymbol{\Phi} = \begin{bmatrix} | & | & & | \\ \phi_1 & \phi_2 & \cdots & \phi_{N_P} \\ | & | & & | \end{bmatrix}, \qquad \boldsymbol{v} = \begin{Bmatrix} v_1 \\ v_2 \\ \vdots \\ v_{N_P} \end{Bmatrix} \tag{9}$$

$\boldsymbol{\Phi}$ is an $N \times N_P$ matrix whose nth column is the shape vector ϕ_n and $\boldsymbol{v}$ is the N_P-dimensional vector of augmented aerodynamic state variables v_n.

A reduced-order representation of the fluid dynamic and aeroelastic systems can be formulated by substituting Eq. (9) into Eq. (1) [and/or Eq. (7)] and premultiplying by the Hermitian transpose of $\boldsymbol{\Phi}$. For instance,

$$\boldsymbol{\Phi}^H \boldsymbol{A} \boldsymbol{\Phi v} = \boldsymbol{\Phi}^H \boldsymbol{B} \boldsymbol{\xi} \qquad \text{or} \qquad \boldsymbol{\mathcal{A} v} = -\boldsymbol{\mathcal{B}} \boldsymbol{\xi} \tag{10}$$

and

$$\{\boldsymbol{\Phi}^H \boldsymbol{I}\} \begin{bmatrix} \boldsymbol{A} & \boldsymbol{B} \\ \boldsymbol{C} & \boldsymbol{D} \end{bmatrix} \begin{Bmatrix} \boldsymbol{\Phi v} \\ \boldsymbol{\xi} \end{Bmatrix} = \begin{bmatrix} \boldsymbol{\mathcal{A}} & \boldsymbol{\mathcal{B}} \\ \boldsymbol{\mathcal{C}} & \boldsymbol{D} \end{bmatrix} \begin{Bmatrix} \boldsymbol{v} \\ \boldsymbol{\xi} \end{Bmatrix} = \begin{Bmatrix} \boldsymbol{0} \\ \boldsymbol{0} \end{Bmatrix} \tag{11}$$

If the Ritz approximation is a good one, that is, N_P is much less than N with no essential loss in accuracy, then Eqs. (10) and (11) will be much smaller models of the original fluid dynamic [(Eq. (1)] and aeroelastic [Eq. (7)] systems that can be quickly assembled and readily solved using conventional eigenvalue techniques.

As will be shown in the following, $N_P \ll N$, and Eqs. (10) and (11) thus represent much smaller models for the original fluid dynamic and/or aeroelastic systems that can be readily assembled and examined using conventional eigenvalue techniques.

The next question becomes what are good choices for the Ritz vectors ϕ_n that will in fact result in good Ritz approximations. Previous detailed studies[2,3] have demonstrated that shape vectors derived via the proper orthogonal decomposition technique[5–7] are an excellent choice. For the sake of brevity, the details are omitted here. However a discussion of how the shapes are derived can be found in Refs. 2 and 3. First, an ensemble of solution snapshots are computed from the original CFD model for several discrete frequencies and structural motions of interest. From this ensemble of solution vectors, the POD shapes are easily derived by solving a small (the size of the number of snapshots) eigenvalue problem. Typically the first few dozen POD modes describe the most dominant dynamic characteristics of the fluid dynamic system, and as such, the POD shapes have proven to be an excellent set of Ritz vectors for fluid dynamic and/or aeroelastic models.

Model Problem

The configuration under consideration is the AGARD model 445.6 wing.[8,9] This is a 45-deg quarter chord swept wing based on the NACA 65A004 airfoil section that has an aspect ratio of 3.3 (for the full span) and a taper ratio of $\frac{2}{3}$. Figure 1 illustrates the computational mesh employed for this configuration. The grid is an O–O topology that employs 49 computational nodes about each airfoil section, 33 nodes normal to the wing, and 33 nodes along the semispan. The total number of fluid dynamic DOF for this CFD mesh is, thus, 266,805. The outer boundary of the grid extends five semispans from the midchord of the wing root section. The particular structural configuration of the wing under consideration is referred to as the "2.5 ft. weakened model 3" (Refs. 8 and 9).

Figure 2 shows the computed wing surface and symmetry plane steady flow pressure contours for the background flow freestream Mach numbers of $M_\infty = 0.960$ and 1.141. A relatively weak shock can be seen at the trailing edge for $M_\infty = 0.960$. This shock appears to get stronger at $M_\infty = 1.141$. The wing section is quite thin (4%), and so a strong shock is not anticipated. When contours are compared, our flowfields look very similar to those of Lee-Rausch and Batina,[10] although they employed a finer mesh.

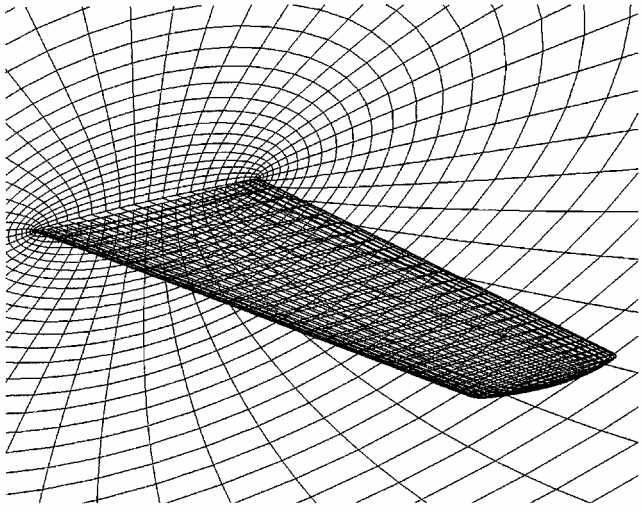

Wing surface and symmetry plane grids

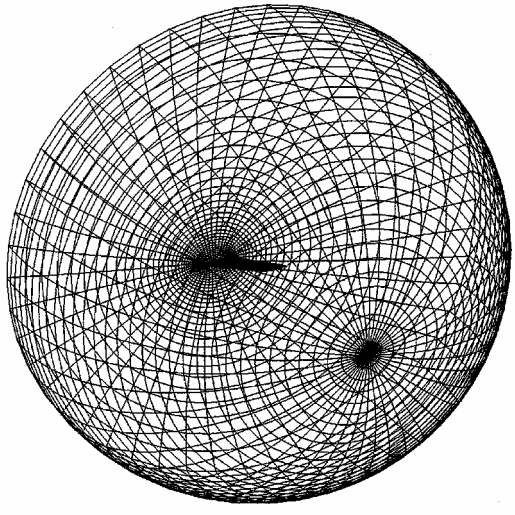

Outer boundary grid

Fig. 1 AGARD 445.6 wing grid topology.

Flutter Results

Figure 3 shows the eigenvalue root loci for various steady background flow Mach numbers. The "gain" for the root loci is the mass ratio or, equivalently, the reduced velocity for a fixed physical velocity. Solution snapshots are computed for the first five given wing structural mode shapes[8] for reduced frequencies from $\bar{\omega} = 0.0$ to $\bar{\omega} = 0.5$ in $\Delta\bar{\omega} = 0.1$ increments. This particular structural configuration flutters for reduced frequencies less than 0.5, thus, making solution snapshots for $\bar{\omega} > 0.5$ unnecessary. If an estimate of the reduced frequency of flutter is not available in advance, one can select a relately small number of reduced frequencies over a wide frequency range to obtain an inital estimate and then add snapshots for more reduced frequencies as needed.

Including the complex conjugate solutions for the corresponding negative-valuedreduced frequencies in the overall ensemble results in a total of 55 available POD shape vectors. In Fig. 3, the curves represent the eigenvalues corresponding to the primarily structural natural modes as mass ratio is varied. Our method also determines the aeroelastic modes originating from the fluid dynamic modes of the POD/ROM. For the range of mass ratios ($0 \le \mu \le 300$) considered in these parametric analyses, the fluid dynamic modes are very damped and, as such, lie to the left and outside of the eigenspectrum range shown. As can been, for each of the Mach numbers, the first structural mode tends to be the critical flutter mode. For the highest Mach number, however, the third structural mode can go unstable if the mass ratio is sufficiently large. Also from Fig. 3, it can be seen that it is unnecessary to use all 55 of the available POD shapes. If

fact, with less than one-half of the POD modes (25 for instance), well-converged results (in the sense of POD/ROM expansion modal refinement) can be achieved.

Figure 4 shows the computed POD/ROM flutter speed and flutter frequency ratios, along with experimental data[8] and data from two other computational methods[10,11] as a function of Mach number. As can be seen, using the POD/ROM methodology one can predict the well-known transonic flutter speed dip, and our results are all within the same tolerance to the experimental results as the other computational methods. Gupta[11] does show better agreement with experiment at the two supersonic Mach numbers, and Gupta attributes this better agreement to better CFD grid refinement.

As a check on mesh convergence, we examined three different grid resolutions for $M_\infty = 1.141$. Table 1 gives the mesh sizes and the corresponding computed flutter reduced velocities:

As can be seen, the results are changing only slightly for each mesh refinement. The $65 \times 49 \times 49$ mesh in fact corresponds to a

Table 1 Mesh resolution convergence trend

Mesh size	V_f
$33 \times 25 \times 25$	0.6421
$49 \times 33 \times 33$	0.6591
$65 \times 49 \times 49$	0.6653

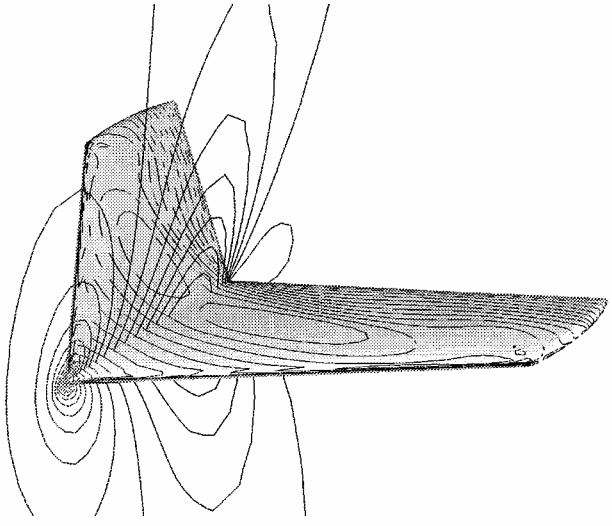

$M_\infty = 0.960$

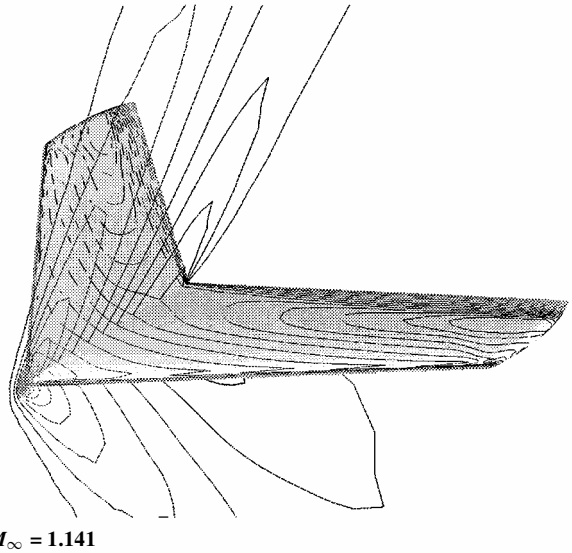

$M_\infty = 1.141$

Fig. 2 AGARD 445.6 wing surface and symmetry plane pressure contours.

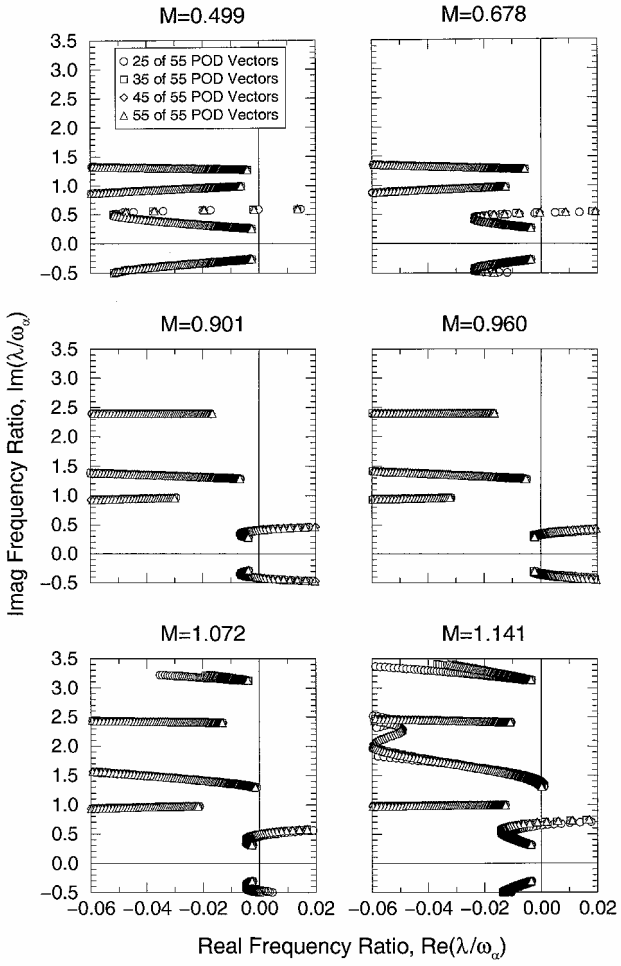

Fig. 3 Aeroelastic root loci at various Mach numbers for the AGARD 445.6 wing weakened configuration, $\alpha_0 = 0.0$ deg.

CFD model with 780,325 DOF that can be reduced to a system with remarkably only 55 DOF. Note that our results do not match the Yates et al.[8] experimental ($V_f \approx 0.41$) or Gupta's[11] computational ($V_f \approx 0.40$) results. However our result matches almost exactly the computational result of Lee-Rausch and Batina.[10] At other Mach numbers, there are more modest differences among all of the methods. Thus, our conclusion is that the differences among the various computational methods are also most likely due to the different CFD methods and grid layouts used, rather than grid refinement alone.

Figure 5 again shows the computed POD/ROM flutter speed and flutter frequency ratios as a function of Mach number. In this instance, however, the flutter results are shown for various numbers of POD modes or Ritz vectors retained in the ROM. As can be seen, even with as few as one-half of the available shapes, well-converged results are obtained. However, note there is somewhat greater sensitivity to the number of POD/ROM modes retained at the supersonic Mach numbers.

Use of Alternate Modal Excitations for Snapshots

As mentioned, one of the key concerns about using the POD/ROM method for three-dimensional configurations has been whether or not an entire set of solution snapshots must be computed for each possible structural configuration of interest. That is, consider an equivalently shaped wing that has a different structural definition, which in turn means different wing vibratory structural mode shapes. The question is whether or not one has to compute a whole new ensemble of solution snapshots based on these new structural motions to do a flutter analysis for the new wing structural definition. Fortunately, only a small number of solution snapshots based on the new modal structural motions will need to be computed. The solution snapshots computed from a previous wing structural definition can

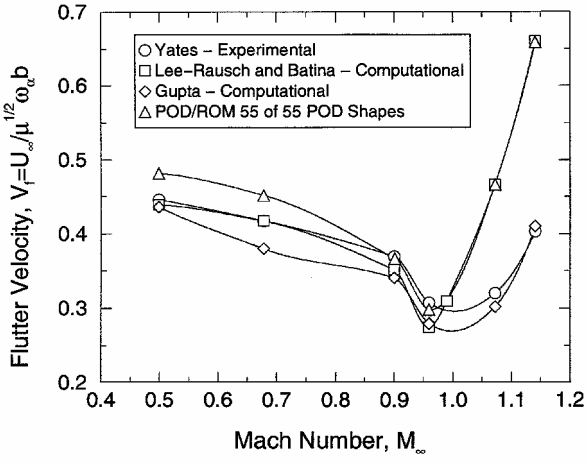

Flutter speed

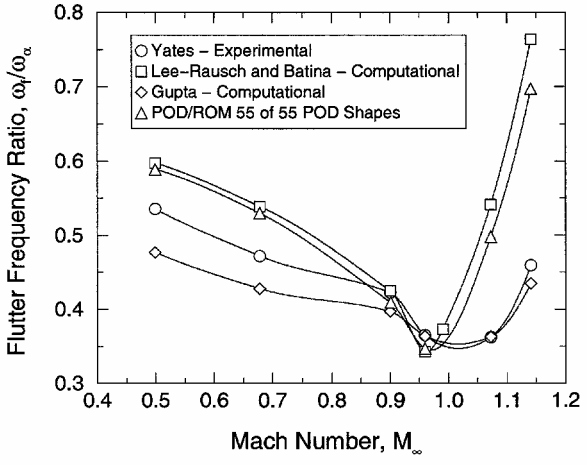

Flutter frequency ratio

Fig. 4 Mach number flutter trend for the AGARD 445.6 wing weakened configuration, α_0 = 0.0 deg.

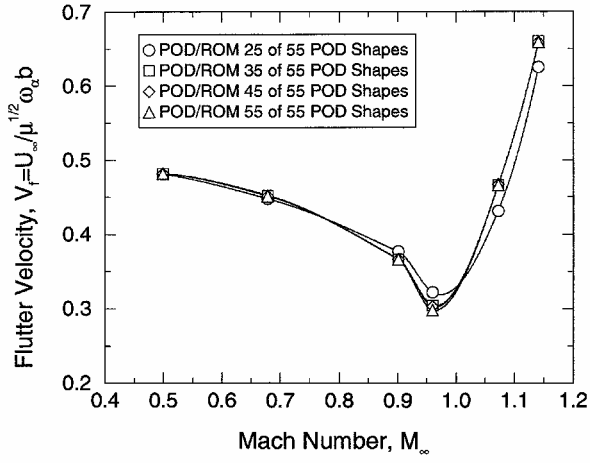

Flutter speed

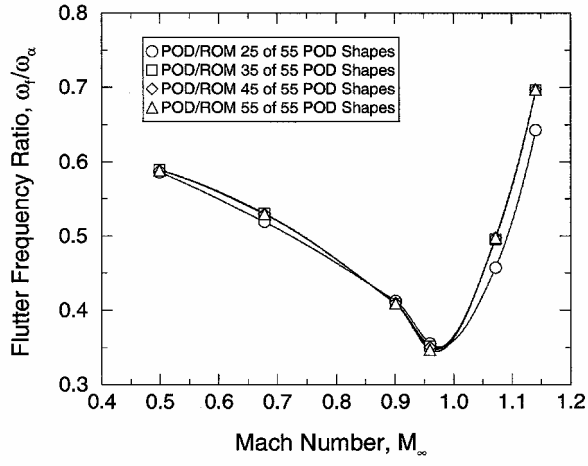

Flutter frequency ratio

Fig. 5 POD/ROM shape vector refinements characteristic for Mach number flutter trend for AGARD 445.6 wing weakened configuration, α_0 = 0.0 deg.

still be used, together with the limited number of solution snapshots for the new structural definition, to generate an accurate POD/ROM. Figure 6 demonstrates this proceedure.

Figure 6a shows the real and imaginary parts of the coefficient of the generalized aerodynamic force corresponding to the first mode pressure acting through the first mode shape as a function of reduced frequency at a Mach number of 0.960. The coefficient of the generalized aerodynamic force is given by

$$E_{i,j}(\bar{\omega}) = -\frac{1}{q_\infty c_r^2}\int\int_A \psi_i p_j(\bar{\omega}) n_z \, dA \tag{12}$$

where the integral is evaluated over the surface of the wing and n_z is z component of the wing surface normal vector, that is, $\hat{\boldsymbol{n}} = n_x\hat{\boldsymbol{i}} + n_y\hat{\boldsymbol{j}} + n_z\hat{\boldsymbol{k}}$ and $\hat{\boldsymbol{n}}$ is oriented such that it points away from the wing surface. In this definition, $p_j(\bar{\omega})$ represents the frequency-dependent unsteady pressure resulting from a wing deformation motion of

$$z/c_r = \psi_i \tag{13}$$

where ψ_i is the ith structural mode shape.

The results for $E_{1,1}$ presented in Fig. 6a are based on the actual solution snapshots and, thus, are what we desire the POD/ROM to be able to model. In Fig. 6b, the POD/ROM of $E_{1,1}$ based on solution snapshots for each of the five structural mode shapes, but only at frequencies of $\bar{\omega} = 0.0$ and 1.0 (for a total of 10 snapshots), is compared to $E_{1,1}$ obtained from the actual snapshots for all frequencies between $\bar{\omega} = 0.0$ and 1.0. As can be seen, the POD/ROM matches at the endpoints of the frequency range as is expected; however this crude POD/ROM performs rather poorly for the intermediate frequencies. Of course, if we use snapshots at all of the frequencies between $\bar{\omega} = 0.0$ and 1.0, the POD/ROM would exactly reproduce the data.

Next, in Fig. 6c, a new POD/ROM for $E_{1,1}$ is shown based on solution snapshots different from the actual mode shapes. These simple wing motion snapshots are for a full wing plunge motion (up/down), full wing pitch about the quarter chord, a first bending type of motion (wing is fixed at the root and the z coordinate component of deflection varies linearly with span), and a first twist type of motion (wing is fixed at the root and the pitch varies linearly with span) for frequencies from $\bar{\omega} = 0.0$ to 1.0 at $\Delta\bar{\omega} = 0.1$ increments for a total of 44 solution snapshots. As can be seen, the POD/ROM in this case also performs very poorly. However, these solutions are in fact helping to reveal the dynamics of the system. In fact, when one uses these snapshots in combination with the actual structural mode snapshots solely at the endpoints of the frequency range of interest, one gets a POD/ROM that produces very accurate results for $E_{1,1}$ as is evident from Fig. 6d.

Figure 7 shows a comparison of the POD/ROM Mach number flutter trend for two cases, 1) the POD/ROM based on solution snapshots corresponding to the actual modal shapes of the wing and 2) based on snapshots using the simple wing motion mode shapes as discussed in the preceding paragraph. As for the earlier Mach number flutter results (Figs. 4 and 5), the snapshot reduced frequencies range from $\bar{\omega} = 0.0$ to 0.5 in $\Delta\bar{\omega} = 0.1$ increments. Included in this second ensemble of solution snapshots are the snapshots corresponding to the actual mode shapes at the endpoints of the frequency range of interest.

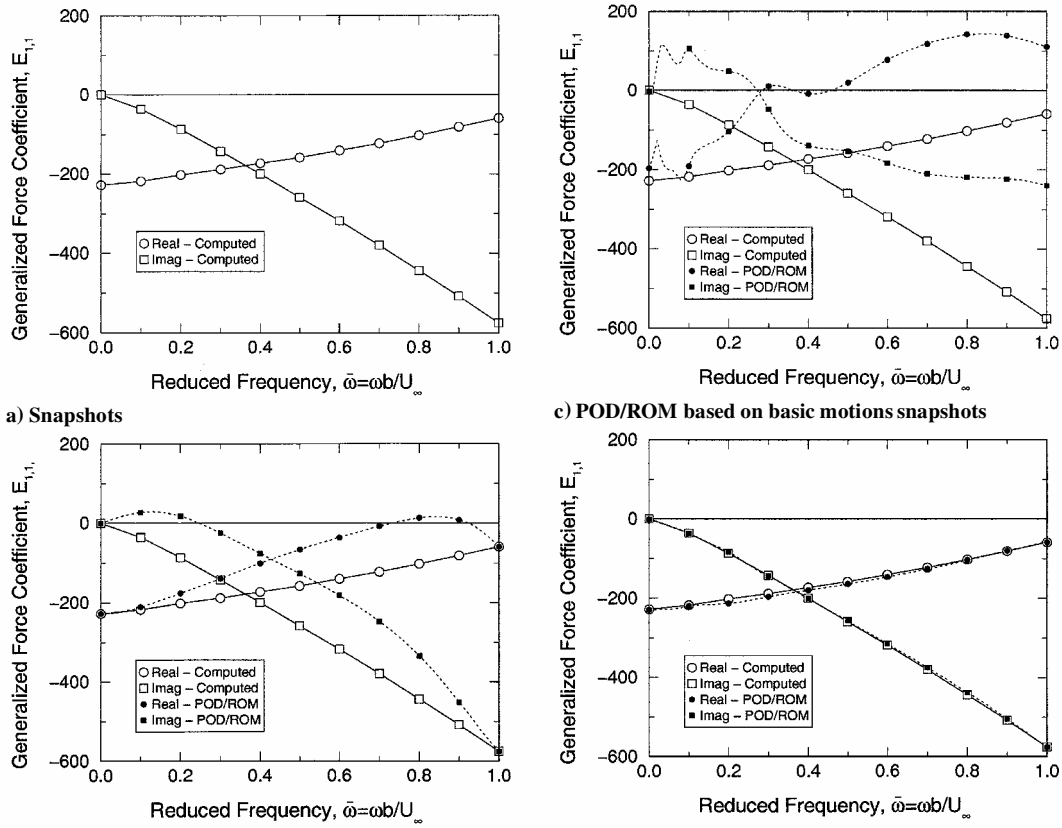

a) Snapshots

c) POD/ROM based on basic motions snapshots

b) POD/ROM based on $\bar{\omega}$ = 0.0 and $\bar{\omega}$ = 1.0 modal snapshots

d) POD/ROM based on $\bar{\omega}$ = 0.0 and $\bar{\omega}$ = 1.0 modal snapshots and basic motions snapshots

Fig. 6 Generalized force modeling with unrelated structural mode shape snapshots.

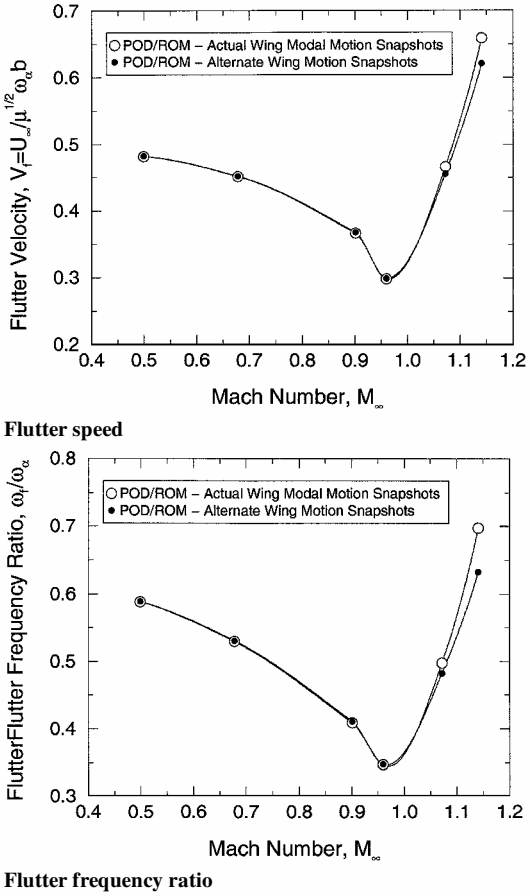

Flutter speed

Flutter frequency ratio

Fig. 7 Mach Number flutter trends using alternate snapshots: AGARD 445.6 wing weakened configuration, α_0 = 0.0 deg.

As can be seen in Fig. 7, one can obtain accurate POD/ROM flutter results using solution snapshots different from the actual wing motions (except at the endpoints of the frequency range of interest) that compare very well to the flutter results based on a POD/ROM model using snapshots corresponding to the actual motions. This is especially true at the lower Mach numbers. There is some difference at the highest Mach number, again suggesting the supersonic case is more sensitive for this wing. The reason the use of alternate modal excitations works is that similar, but not identical, structural modes effectively excite the same most significant fluid dynamic modes.

Finally, we present similar results for a simple two-dimensional configuration. Consider an unsteady NACA 64A010A airfoil configuration that not only undergoes typical plunge and pitch motions (Figs. 8a and 8b), but also has motions where the airfoil mean camber line distorts based on simple trigonometric functions, that is, $z_c(x) = \bar{\sigma}_1 \cos(2\pi x/c)$ (Fig. 8c), $z_c(x) = \bar{\sigma}_2 \sin(2\pi x/c)$ (Fig. 8d), $z_c(x) = \bar{\sigma}_3 \cos(4\pi x/c)$ (Fig. 8e), etc. The initial question was, as one considers each subsequent motion, does one have to include a number of snapshots based on the new motion that is equal to the number of snapshots for each of the previous motions to produce an accurate POD/ROM.

Figure 9 illustrates how, after a sufficient number of snapshots have been included in the snapshot ensemble, only the endpoint frequencies are required for each additional motion. In this instance, the NACA 64A010A airfoil is modeled in a $M_\infty = 0.5$ and $\alpha_0 = 0.0$ (deg) background flow, and shown on the abscissa are increments in the number of overall motions considered. Shown on the ordinate is the order in which the snapshots for each particular motion are added to the overall ensemble. The reduced frequency range of interest is $0.0 \le \bar{\omega} \le 1.0$, and thus the first two snapshots considered for each motion correspond to the endpoints of this frequency range. Further snapshots are added to the ensemble for a given motion to best model the intermediate frequencies.

Shown in Fig. 9 is the accuracy achieved in modeling the airfoil unsteady lift and moment along the paths $\bar{s} = re^{j\theta}$ (where $\theta = 90$, 60, and 120 deg and $0 \le r \le 1$) in the complex reduced

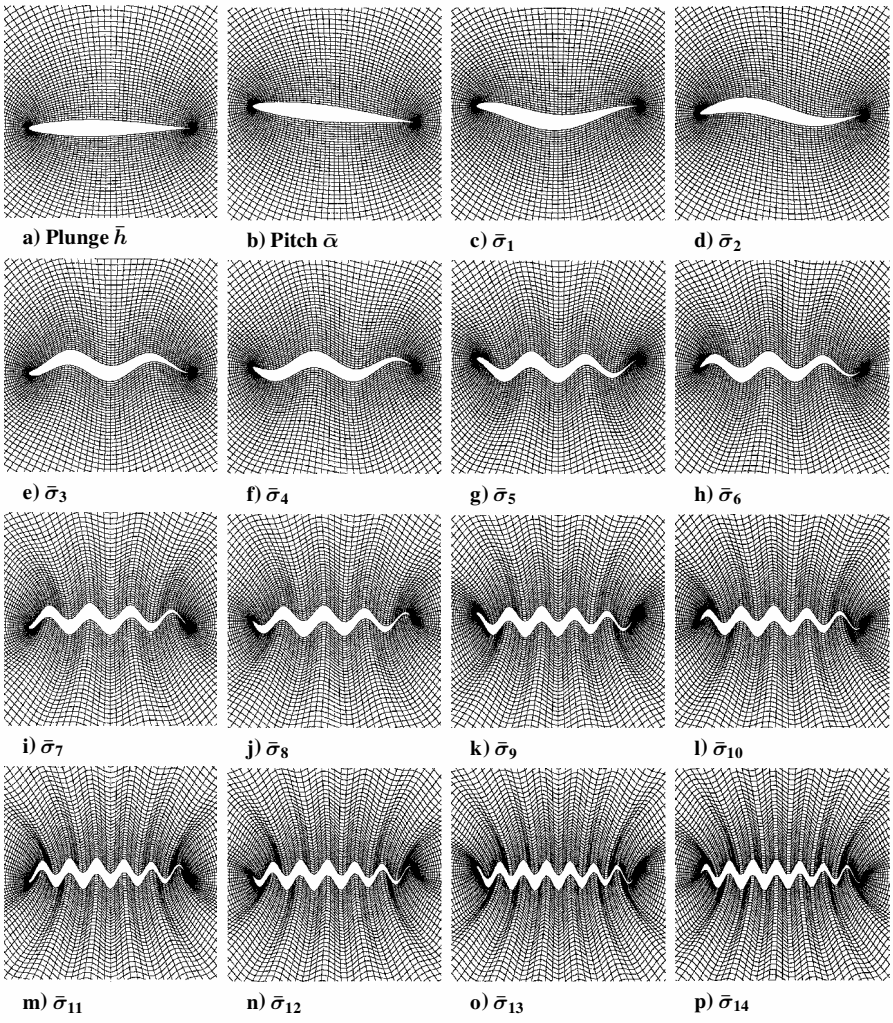

Fig. 8 Airfoil sample motions: NACA 64A010A airfoil section 129 × 65 mesh.

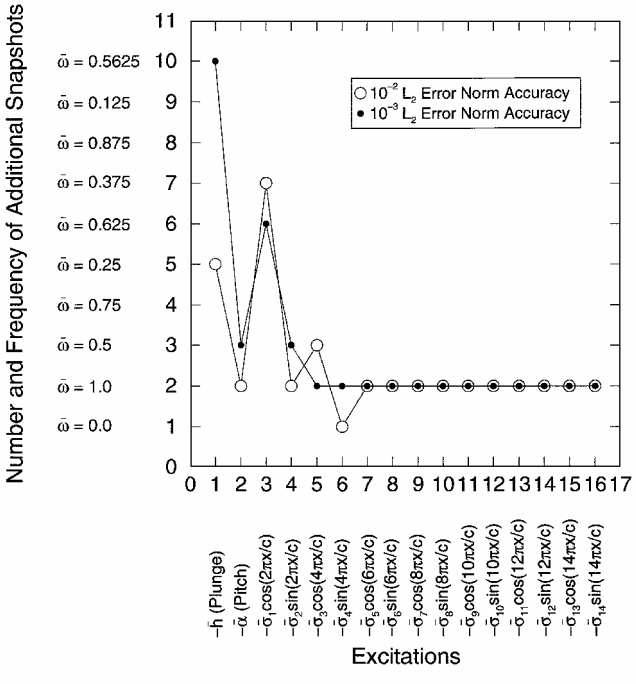

Fig. 9 Additional snapshot requirements to achieve two different levels of accuracy for lift and moment transfer functions along the paths $\bar{s} = re^{j\theta}$, where θ = 90, 60, and 120 deg and $0 \leq r \leq 1$, in the complex reduced frequency $\bar{s}$ plane for nth and all previous motions: M_∞ = 0.5 and α_0 = 0.0 deg.

frequency $\bar{s}$ plane. The curves illustrate the number of snapshots necessary to achieve a given level of accuracy for the nth and all previous motions. The accuracy is based on a comparison to a POD/ROM that is derived from a snapshot ensemble comprising all of the possible motions at all of the possible frequencies. Thus, for example, to achieve a 10^{-3} L_2 norm accuracy when just considering plunge motion, one needs a total of 10 plunge snapshots for the frequency values indicated on the ordinate of the plot.

Next, considering pitch motion, one would then need to add only three pitch motion snapshots corresponding to the frequencies $\bar{\omega} = 0.0$, $\bar{\omega} = 1.0$, and $\bar{\omega} = 0.5$ to the overall ensemble to get 10^{-3} L_2 norm accuracy for now both the pitch and plunge motions. Considering next the first airfoil bending motion $\bar{\sigma}_1$, one would then need to add a total of six $\bar{\sigma}_1$ snapshots to achieve 10^{-3} L_2 norm accuracy for now plunge, pitch, and $\bar{\sigma}_1$ motion. Three $\bar{\sigma}_2$ snapshots would then be needed when also taking in account $\bar{\sigma}_2$ motions, two $\bar{\sigma}_3$ snapshots when considering $\bar{\sigma}_3$ motions, and so on.

As can be seen, Fig. 9 illustrates the interesting result that after a sufficient number of snapshots have been included in the overall ensemble, only the two endpoint frequency snapshots for each subsequent possible motion need be added to the ensemble to maintain a given level of accuracy. Interestingly enough, this appears to be an asymptotic limit. That is, the two endpoint frequency range snapshots always appear to be necessary when considering a large number of motions.

Conclusions

The POD/ROM method has been demonstrated for the flutter analysis of a three-dimensional flow transonic wing configuration. We have shown that the number of ROM DOF necessary to create

accurate models is on the order of a few dozen, as is the case in two-dimensions. We have also shown that it is unnecessary to compute a completely new ensemble of solution snapshots based on the vibratory mode shapes for each new structural configuration that might be under consideration. One can simply compute a set of snapshots based on some basic wing motions at a number of frequencies. Then snapshots only at the endpoints of the frequency range of interest need to be computed for the specific mode shapes of the configuration of interest. These endpoint snapshots lock in the unsteady fluid dynamic characteristics for the particular mode shapes, and the simple motion snapshots then act to resolve the dominant dynamics of the flow throughout the full frequency range of interest. Both of these observations suggest that the POD/ROM methodology will be very useful for design studies of transonic aeroelastic configurations when several structural configurations may be under consideration and where a range of structural and flow parameters must be examined.

Acknowledgments

The authors would like to acknowledge with appreciation the support of Air Force Office of Scientific Research and Program Director, Daniel Segalman, for this work.

References

[1]Kim, T., "Frequency-Domain Karhunen–Loève Method and Its Application to Linear Dynamic Systems," *AIAA Journal*, Vol. 36, No. 11, 1998, pp. 2117–2123.

[2]Hall, K. C., Thomas, J. P., and Dowell, E. H., "Proper Orthogonal Decomposition Technique for Transonic Unsteady Aerodynamic Flows," *AIAA Journal*, Vol. 38, No. 10, 2000, pp. 1853–1862.

[3]Thomas, J. T., Hall, K. C., and Dowell, E. H., "Reduced-Order Aeroelastic Modeling Using Proper-Orthogonal Decompositions," CEAS/AIAA/ICASE/NASA Langley International Forum on Aeroelasticity and Structural Dynamics 1999, June 1999.

[4]Ni, R. H., "A Multiple-Grid Scheme for Solving the Euler Equations," *AIAA Journal*, Vol. 28, No. 12, 1982, pp. 2050–2058.

[5]Loève, M., *Probability Theory*, D. Van Nostrand, New York, 1955.

[6]Lumley, J. L., "The Structures of Inhomogeneous Turbulent Flow," *Atmospheric Turbulence and Radio Wave Propagation*, edited by A. M. Yaglom and V. I. Tatarski, Nauka, Moscow, 1967, pp. 166–178.

[7]Holmes, P., Lumley, J. L., and Berkooz, G., *Turbulence, Coherent Structures, Dynamical Systems and Symmetry*, Cambridge Univ. Press, Cambridge, England, U.K., 1996.

[8]Yates, E. C., Jr., "AGARD Standard Aeroelastic Configurations for Dynamic Response I—Wing 445.6," *Proceedings of the 61st Meeting of the Structures and Materials Panel*, AGARD-R-765, 1985, pp. 1–73; also NASA TM 100492, Aug. 1987.

[9]Yates, E. C., Jr., Land, N. S., and Foughner, J. T., Jr., "Measured and Calculated Subsonic and Transonic Flutter Characteristics of a 45 Deg Sweptback Wing Planform in Air and in Freon-12 in the Langley Transonic Dynamics Tunnel," NASA TN D-1616, March 1963.

[10]Lee-Rausch, E. M., and Batina, J. T., "Wing Flutter Boundary Prediction Using Unsteady Euler Aerodynamic Method," *Journal of Aircraft*, Vol. 32, No. 2, 1995, pp. 416–422.

[11]Gupta, K. K., "Development of a Finite Element Aeroelastic Analysis Capability," *Journal of Aircraft*, Vol. 33, No. 5, 1996, pp. 995–1002.